

# INVESTIGATION OF THE CANLUB/SHEATH INTERFACE IN CANDU FUEL AT EXTENDED BURNUP BY XPS AND SEM/WDX

W.H. HOCKING<sup>(1)</sup>, R. BEHNKE<sup>(2)</sup>, A.M. DUCLOS<sup>(2)</sup>, A.F. GERWING<sup>(2)</sup> and P.K. CHAN<sup>(3)</sup>

<sup>(1)</sup>AECL, Chalk River Laboratories Chalk River, Ontario, Canada K0J 1J0

<sup>(2)</sup>AECL, Whiteshell Laboratories, Pinawa, Manitoba, Canada R0E 1L0

<sup>(3)</sup>AECL, Sheridan Park, 2251 Speakman Drive, Mississauga, Ontario, Canada L5K 1B2

## ABSTRACT

A systematic investigation of the fuel-sheath interface in CANDU fuel as a function of extended burnup has been undertaken by XPS and SEM/WDX analysis. Adherent deposits of  $\text{UO}_2$  and fission products, including Cs, Ba, Rb, I, Te, Cd and possibly Ru, have been routinely identified on CANLUB coated and bare Zircaloy surfaces. Some trends in the distribution and chemistry of key fission products have begun to emerge. Several potential mechanisms for degradation of the CANLUB graphite layer at high burnup have been practically excluded. New evidence of carbon relocation within the fuel element and limited reaction with excess oxygen has also been obtained.

## 1. INTRODUCTION

Stress-corrosion cracking (SCC) of the Zircaloy sheath used on  $\text{UO}_2$  fuels in water-cooled nuclear reactors was first recognized over three decades ago [1]. Fission-product iodine was subsequently identified as the probable causative agent, although cesium and cadmium, especially in combination, remain suspect as well [1-3]. The incubation period for SCC of Zircaloy in out-reactor experiments has been shown to be less if the iodine is initially present in the form of volatile  $\text{ZrI}_4$  rather than  $\text{I}_2$ , which will react with Zr to form the series of compounds  $\text{ZrI}_n$  with  $n = 1, 2, 3$  and  $4$  [4-6]; however, even CsI can ultimately be effective, particularly under irradiation, and despite being thermodynamically stable with respect to formation of  $\text{ZrI}_4$  by reaction with Zr metal [1,7,8]. Access of iodine, or any other agent, to the crack has therefore been inferred to be more important than its original chemical form [1].

The term pellet-cladding interaction (PCI) is commonly applied to the phenomenon as well, reflecting the role of the exact fuel-sheath configuration in creating the requisite high local stress intensities through thermal expansion and fission-gas release [1]. Defect thresholds for maximum element power and change in power over a short period, which decrease with total burnup as the inventory of the SCC agents increase, have been empirically determined [1]. They are dependent on the details of the fuel design, including the pellet geometry, whether there is a fuel-sheath gap and the presence of a barrier layer. A thin coating of elemental zirconium has been shown to provide extended protection against PCI failure for LWR fuel, which has a thick-

walled, free-standing Zircaloy cladding [1]. If a defect does occur, however, by SCC or any other mechanism, rapid hydriding of this layer can lead to axial splitting of the fuel element [9,10].

The thin-walled Zircaloy sheath used for CANDU fuel, which collapses onto the  $\text{UO}_2$  pellets under the coolant pressure, was initially found to be quite susceptible to SCC — producing an epidemic of fuel failures during the early operation of reactors at Douglas Point and Pickering [1,11]. Introduction of the CANLUB graphite coating on the interior sheath surface virtually eliminated the problem for typical burnup and power of the natural uranium fuel in a CANDU reactor. Although graphite is effective as a pellet lubricant in reducing in-reactor stress, the CANLUB layer has been shown to play a more important role as a fission-product chemical barrier; however, the mechanisms involved remain obscure [1-3,12]. Organic residues in the CANLUB layer have recently been proposed as the key ingredient [13], which might facilitate iodine immobilization through formation of stable cluster compounds of the type  $\text{Zr}_6\text{I}_{12}\text{C}$ ,  $\text{Zr}_6\text{I}_{14}\text{C}$  and  $\text{MZr}_6\text{I}_{14}\text{C}$ , where M is Rb or Cs [14,15]. There is also some evidence that CANLUB influences the evolution of the oxygen potential in CANDU fuel at high burnup, by inhibiting reaction of fission-liberated oxygen with the sheath [16,17]. Severe degradation of the integrity of the CANLUB layer with extended burnup has now been well documented; however, the processes involved are completely unknown [17,18]. Fission-gas releases beyond the levels predicted by existing fuel-performance codes and significantly increased fuel-failure rates have been observed for such fuels as well.

A systematic investigation of the chemistry and microstructure across the CANLUB/sheath interface in CANDU fuel at extended burnup has been undertaken by X-ray photoelectron spectroscopy (XPS) and scanning electron microscopy (SEM) with wavelength dispersive X-ray (WDX) analysis. Sheath, end-cap and plenum-spacer surfaces in three Bruce-type CANDU fuels (37 element bundle) that had been irradiated to high burnup in the NRU research reactor have now been characterized; inner elements, without CANLUB, as well as outer elements, with CANLUB, were analyzed for comparison. An outer element from a CANDU power-reactor fuel with a normal burnup was also examined for reference. The focus in this paper is on recent results from the highest burnup (950 MW·h/kg U) Bruce-type fuel.

## 2. EXPERIMENTAL PROCEDURES

Power histories and other relevant information on the CANDU fuels from which the sheath has been removed for characterization by XPS and SEM/WDX are summarized in Table 1. Because of the high surface specificity of XPS, precautions were required to minimize surface alteration or contamination; in particular, flowing argon was used for cooling and protection throughout. Complete element segments, 1-3 cm long, were cut first using a high-speed silicon-carbide saw. The already cracked fuel was then easily removed by gentle tapping, without causing appreciable damage to the interior surfaces. Finally, appropriate samples, typically ~5 mm wide by ~7 mm long, were cut using a slow-speed diamond saw operated with minimum pressure. All samples were affixed to Al mounts using Ag-based epoxy and analyzed by XPS without prior chemical or physical treatment.

X-ray photoelectron spectra were recorded using a modified McPherson ESCA-36 instrument that has been equipped with a position-sensitive detector (PSD) and specifically adapted for studies of highly radioactive materials [19,20]. Photoelectron emission was excited by Mg K $\alpha$  characteristic radiation. The spectrometer dispersion and work function were routinely calibrated using gold and copper standards with the binding-energy scale referenced to the Fermi level [21]. Because of the focussing properties of the spectrometer, photoelectrons were collected from a narrow strip,  $\sim 400$   $\mu\text{m}$  wide, down the centre of the sample. The length of this strip was adjusted to less than that of the sample, by setting an electronic PSD aperture. Information on the near-surface composition as a function of depth was compiled by sequential XPS analysis and argon-ion sputtering using a Kratos Mini Beam I ion gun. The focussed 3 keV ion beam, which was incident on the sample at  $45^\circ$  to the surface normal, was rastered over the whole area to provide an average current density of  $0.7 \mu\text{A}/\text{cm}^2$ . Under these conditions a sputtering rate of 0.1 nm/min has been previously derived from ion-implanted  $\text{UO}_2$  [22].

The surface morphology of each sample was subsequently examined by secondary electron imaging using an Hitachi model S-570 SEM [23]. A thin film of gold was sputtered onto the sample to prevent surface-charging artefacts under the electron-beam interrogation. Selected features were identified by WDX analysis using a Microspec 2A four-crystal x-ray spectrometer.

### 3. RESULTS AND DISCUSSION

#### 3.1 Overview of Trends with Burnup

The chemistry and microstructure across the CANLUB/sheath interface with the  $\text{UO}_2$  pellets in CANDU fuel has been found to progressively change as a function of burnup. An essentially intact coating of CANLUB is visible in secondary electron images (Figure 1) collected from the Y00005Z/4 (normal-burnup CANDU power-reactor fuel) sheath samples, although the mottled appearance indicates local variations in thickness. X-ray microanalysis of the fine particulate material, which seems to collect in the hollows, revealed only U and Zr (not sensitive to C and O) consistent with fuel and thinly coated or exposed sheath. At higher burnup (BDL-406-XY/11 and BDL-406-AAH/8), the area still coated with identifiable CANLUB — featureless patches with a smooth texture — was much reduced; instead, extensive coverage by nodular/filamentary structures of increasing complexity was observed (Figure 1). Again, X-ray microanalysis showed mainly U and Zr, but now with some fission products, most notably Cs. The distinctive appearance of these structures is indicative of *in situ* growth rather than simple accumulation of debris. Because of the relatively low temperatures near the sheath, radiation-enhanced processes likely play a significant role. At the highest burnup (BDL-406-GF/2) there were no longer any recognizable patches of CANLUB and the adherent deposits had evolved into a dense mat of diverse morphology, as illustrated in Figure 2. Cesium and barium were now commonly more prominent than U and Zr in the X-ray microanalyses, which also detected lesser amounts of other fission products, notably I and Te.

Representative X-ray photoelectron spectra collected from the CANLUB/sheath surfaces of the same four fuels have been reproduced in Figure 3 (normalized to the C 1s peak). For the

Y00005Z/4 sheath, the dominant peak arises from carbon (C 1s), reflecting the presence of a still largely intact CANLUB layer. The modest N 1s peak as well as part of the intensity in the O 1s signal can be attributed to adsorbed surface contamination, which is enhanced by radiolysis effects during air exposure [24]. Minor U 4f and Zr 3d peaks are consistent with a small amount of adherent fuel and a little exposed sheath respectively. Although it is not evident from the Y00005Z/4 spectrum in Figure 3, Cs was just detectable on the normal-burnup sheath, but otherwise fission products had not begun to accumulate. At higher burnup (BDL-406-XY/11 and BDL-406/AAH/8), the relative proportions of U and Cs have increased significantly and several other fission products were commonly detected as well. The low intensity of the Zr 3d doublet here indicates that any sheath exposed by degradation or loss of CANLUB has been largely re-coated with fuel and fission products. A reversal in the trend of increasing U 4f peak intensity has been observed at the highest burnup (BDL-406-GF/2); however, as shown below, this can be attributed, at least in part, to formation of a surface film enriched in fission products, notably Cs, which now provides the strongest photoelectron emission.

The interior surfaces of the end caps on these four fuel elements were also characterized by SEM/WDX and XPS. Adherent deposits were clearly observed in all of the secondary-electron images — typically with an undistinguished, fine-grained appearance, rather than the distinctive morphologies seen on the sheath surfaces above. Elevated levels of fission products, notably Cs, were also detected, surprisingly, even at the low burnup (Y00005Z/4). Although the end caps had not been intentionally coated with CANLUB, carbon was nonetheless consistently found by XPS in comparatively high abundance. Further details of the surface composition for the highest burnup fuel are provided in the following sub-sections.

### 3.2 Fission-Product Distributions at High Burnup

Key segments of the X-ray photoelectron spectra (normalized to the C 1s peak) recorded from four BDL-406-GF/2 samples — an end cap, a plenum spacer and two pieces of sheath — are compared in Figure 4. In each case, the analyzed surface originally faced toward the fuel, with the end cap having been separated from it by the height (~1 cm) of the plenum spacer volume, and was in the as-exposed condition. Significant levels of fission products, including Cs, Ba, Rb, I, Te and Cd, have been found on these surfaces, although there are clearly some differences in the relative abundances. The presence of Cs appears to be somewhat biased toward sheath over plenum-spacer and especially end-cap surfaces, which indicates a restricted mobility that would be incompatible with predominance of the elemental state ( $mp = 28.4^{\circ}\text{C}$ ) and probably even the binary metal oxides [15,25,26]. A converse argument could be made above for the low-burnup fuel and together these observations may point toward evolution of the cesium chemistry with burnup, possibly because of an increase in the oxygen potential. The widespread distribution of iodine similarly does not support as the main species volatile  $\text{I}_2$  or  $\text{ZrI}_4$ , which has an appreciable vapour pressure above Zr surfaces exposed to  $\text{I}_2$  at sheath temperatures [4-6]; either would be expected to accumulate on the cooler end cap as the less volatile lower iodides. Conversely, Rb was found at only modest levels on the sheath and plenum-spacer surfaces but displaces Cs as the dominant fission product on the end cap. This presumably reflects enhanced volatility of Rb and could be a useful constraint on potential reaction schemes or decay chains [20,27]. The detection of Cd only at the end of the element, on the plenum spacer and end cap, suggests transport in an

elemental form (mp = 321°C) or possibly as CdI<sub>2</sub> (mp = 387°C), because of the involatility of the oxides [25]. There does not appear to be much that can be inferred from the relatively wide distribution of Ba and Te at quite modest abundance. The observation of Cl, most notably on sheath sample #2, likely reflects a high degree of segregation of a minor impurity from the UO<sub>2</sub> and/or the CANLUB. X-ray photoelectron spectra were also recorded from these samples after increasing intervals of argon-ion sputtering — illustrative examples are displayed in Figure 5 and the results are discussed further below. A destructive examination of a second outer element from the same fuel bundle, which is currently in progress (BDL-406-GF/3), has been providing similar findings, except for distinctly higher levels of Ba.

### 3.3 Fission-Product Chemistry at High Burnup

The binding energies determined for the major photoelectron peaks of the various fission products are summarized in Table 2. As-received and sputtered surfaces have been distinguished to help assess any changes caused by air exposure or argon-ion bombardment; however, measurements for the four samples and at different sputter times, which both showed only slight, random variations, were averaged. Compensation for surface charging was based on the C 1s peak (at 285.0 eV) and the U 4f<sub>7/2</sub> peak (at 380.0 eV after sputtering), but other core levels, notably Zr 3d<sub>5/2</sub>, N 1s and O 1s, were used to check for internal consistency as well [20,24]. Typical charging corrections were only 0.2-0.4 eV, except for sheath sample #2 where they exceeded 4 eV. The binding energies determined before and after sputtering are sufficiently close for all of the fission products, aside from tellurium, to indicate that at least the valence has not changed.

Chemical-shift effects indicate a +1 valence for Cs and Rb and a -1 valence for I and Cl [20,26,28-34]. Atomic intercalation in graphite can be ruled out for the alkali metals (Cs 3d<sub>5/2</sub> = 275.8 eV, Rb 3p<sub>3/2</sub> = 239.8 eV) as well as the elemental state (Cs 3d<sub>5/2</sub> = 726.3 eV, Cs 4d<sub>5/2</sub> = 77.5 eV, Cs α' = 1296.6 eV, Rb 3d<sub>5/2</sub> = 112.0 eV and Rb 3p<sub>3/2</sub> = 239.1 eV). Neither would be expected to occur in the operating fuel [35] and in any case both should oxidize upon exposure to air [26,30]. Identification of the -1 valence for Cl and I supports the inference above that they are not in a highly labile form, such as I<sub>2</sub> adsorbed in the graphite (I 3d<sub>5/2</sub> = 620.5 eV [36]), with the caveat of possible fractional release upon air exposure. The various zirconium iodides would all rapidly oxidize to ZrO<sub>2</sub> and I<sub>2</sub> upon exposure to the atmosphere [15,37], whereas the carbon-centered cluster compounds Zr<sub>x</sub>I<sub>y</sub>C are reported to be air-stable [14]. The location of the Zr 3d doublet (Zr 3d<sub>5/2</sub> = 182.2-182.6 eV) always indicated that zirconium was predominantly in the tetravalent state, consistent with ZrO<sub>2</sub> or a zirconate [29,35]; however, a minor contribution from a lower valent species, such as Zr<sub>x</sub>I<sub>y</sub>C, could easily have been obscured by weak Ba 4p<sub>3/2</sub> photoemission, which occurs at a similar binding energy (Zr 3d<sub>5/2</sub> = 179-180 eV) [29,38,39]. A comprehensive early investigation [31] of the alkali metal halides yielded lower binding energies for CsCl and CsI (but not RbCl or RbI) than those in Table 2, by ~1 eV; however, more recent studies [28,32-34] have reported measurements that are in much close agreement with the present results (I 3d<sub>5/2</sub> = 618.8-619.3 eV, Cs 3d<sub>5/2</sub> = 724.7-724.9 eV and Cs α' = 1293.9 eV for CsI and Cs α' = 1293.6 eV for CsCl). Because the cesium chemical-shift effects for Cs<sub>2</sub>O, CsOH and even the uranates are not much different [20,26,33], a mixture of alkali metal halides and oxides could be easily accommodated, consistent with the excess of Cs and Rb over Cl and I.

Distinguishing between oxidized and elemental Ba using XPS is difficult, because the Fermi level can be shifted within the bandgap by defect states [40]; in the present case, only the divalent species is plausible [35]. The binding energy determined for the strongest Te 3d<sub>5/2</sub> peak before sputtering (Table 2) falls just above values published for TeO<sub>2</sub> (575.7-576.1 eV) and TeL<sub>4</sub> (575.8 eV), whereas a range of numbers reported for TeO<sub>3</sub> and Te(OH)<sub>6</sub> extend ~1 eV toward higher energy [28,29]. A second, weaker photoelectron emission structure was also apparent from the outset, with a Te 3d<sub>5/2</sub> binding energy that is characteristic of elemental tellurium (573.0 eV) [28,29]; after argon-ion sputtering all of the intensity was shifted into the latter. This behaviour could simply reflect preferential sputtering [20]; however, detection of some elemental Te even initially suggests instead removal of a thin oxide film formed by air exposure. The Cd 3d<sub>5/2</sub> binding energies reported Cd(OH)<sub>2</sub> (405.0 eV), CdI<sub>2</sub> (405.4 eV) and elemental Cd (405.1 eV) are practically the same and agree well with the present result (Table 2), whereas the binary oxides, CdO (404.2 eV) and CdO<sub>2</sub> (403.6 eV), which exhibit anomalous negative chemical shifts, can be reasonably excluded [20,28,29]. An elemental state, or possibly the iodide, would then seem most likely, based on both the distribution as discussed above and the fuel chemistry [35].

### 3.4 Quantitative XPS Analyses

All of the X-ray photoelectron spectra recorded from the four BDL-406-GF/2 samples were quantitatively analyzed following the standard XPS theory for uniform composition over the escape depth of the photoelectrons [28]. Integrated peak areas were normalized by the photoionization cross-section,  $\sigma$ , and  $E^{3/2}$ , where E is the electron kinetic energy. The spectrometer transmission function has been shown to be a linear function of E and the electron escape depth has been assumed to have an  $E^{1/2}$  dependence [19,41]. Photoionization cross-sections derived from extensive measurements on an instrument operated in the same (non-retarding) mode were used [41]; the  $\sigma$  value for U 4f is probably the least reliable [20]. Further details of the analysis procedure and the uncertainties involved have been previously discussed [19,20]; the results are collected in Table 3. Because of the pronounced surface roughness, these data cannot be interpreted as true composition depth profiles, rather they merely provide an indication of whether an element is surface enriched or depleted. Both Cs and Rb slowly decrease with sputter time, although there is some variability in the extent (c.f. trends on sheath and end-cap surfaces). Conversely, both Ba and I consistently increase with sputtering, the latter more so on sheath than end-cap or plenum-spacer surfaces. Differences in interfacial chemical reactions as well as migration rates and radioactive decay chains likely contribute to these divergent fission-product distributions. Systematic increases in the uranium and zirconium with sputtering can be reasonably attributed to overcoating of transferred fuel structures and exposed Zircaloy by a thin fission-product film. The low uranium abundance on the end cap is consistent with negligible volatility at typical sheath temperatures for the likely uranium compounds.

### 3.5 CANLUB Chemistry and Degradation at High Burnup

Conventional post-irradiation examinations of CANDU fuel at extended burnup have previously shown low retention of the CANLUB layer — at least in its original form [18]. This is consistent with the progressive alteration of the microstructure across the CANLUB/sheath

interface, as revealed by secondary electron images (Figures 1 and 2). Conversely, the quantitative XPS analyses have confirmed that carbon remains the main constituent on the sheath surfaces from CANLUB coated fuel elements even at high burnup (Table 3), although the similar or even larger proportions of carbon found on end-cap and plenum-spacer surfaces point toward some relocation to the cooler region. In all cases the binding energy determined for the C 1s peak (charge referenced to U 4f<sub>7/2</sub> or Zr 3d<sub>5/2</sub>) was indicative of predominantly C-C/C-H bonding, graphite and/or hydrocarbon, consistent with the original CANLUB formulation [1]. Nonetheless, formation of the carbon-centered cluster compounds (Zr<sub>6</sub>I<sub>12</sub>C, Zr<sub>6</sub>I<sub>14</sub>C and MZr<sub>6</sub>I<sub>14</sub>C with M = Cs or Rb) remains a possibility, because the low carbon content involved would be hard to distinguish. The converse depth distributions of I and Cs/Rb certainly suggest some difference in chemical association.

Asymmetry on the high-binding energy side of the C 1s peak, which can develop into secondary structure that might be correlated with burnup, indicates a modest contribution from oxygenated functional groups [29]. Because this persists throughout the sputtered depth, as illustrated in Figure 5 for BDL-406-GF/2 Sheath #2, it cannot be just a surface phenomenon or artefact from the brief air exposure [24]. Some reaction of oxygen with carbon would appear to be needed for chemical balance from the quantitative XPS analyses (Table 3) as well. Conversely, appreciable oxidation of carbon to CO<sub>2</sub> is not supported by mass spectrometric analysis of the gas in the element void space. A small peak near 280.0 eV can be reasonably assigned to the Ru 3d<sub>5/2</sub> core level of elemental ruthenium (although confirmation is lacking as the Ru 3d<sub>3/2</sub> component is then buried under the main C 1s peak) rather than a chemically shifted carbide species. The C 1s binding energy of ZrC at 281.5 eV [42,43] would appear to be typical of metal carbides, for which the range 281-283 eV is given in the XPS handbook [29]. There is also no convincing evidence of carbide formation from chemical-shift effects for any of the metal core levels, in particular Zr 3d and U 4f. Thus, bulk reaction of the graphite with either the sheath or the fuel can be practically excluded.

Decreased mechanical integrity of the CANLUB layer, leading to physical loss during preparation of metallographic cross-sections is now considered a more plausible explanation for the low retention [44]. Severe radiation damage of the graphite as well as any residual organic compounds by fission fragments (and  $\alpha$ ,  $\beta$ ,  $\gamma$  and neutron radiation) would be consistent with this hypothesis. Fission products created near the pellet surface and emitted normal to it would have sufficient energy to completely transit a typical CANLUB film [45,46]. At a minimum, disruption of the initially large graphite sheets into progressively smaller fragments could be expected and might even lead to the formation of buckminsterfullerenes, which can sublime at typical sheath temperatures [47,48]. Such alterations would facilitate relocation of carbon within the fuel element (e.g., to end caps) and could explain the observed degradation of CANLUB properties at high burnup, including reduced protection against SCC. Introduction of increasing amounts of fission-freed oxygen, fuel and fission products, through migration and recoil implantation, can only augment the process.

## REFERENCES

1. COX B., "Pellet-Clad Interaction (PCI) Failures of Zircaloy Alloy Fuel Cladding —A Review", *J. Nucl. Mater.* 172, 249-292 (1990).
2. WOOD J.C., "Factors Affecting Stress Corrosion Cracking of Zircaloy in Iodine Vapour", *J. Nucl. Mater.* 45, 105-122 (1972/73).
3. CUBICCIOTTI D., S.M. HOWARD and R.L. JONES, "The Formation of Iodine-Induced Stress Corrosion Cracks in Zircalloys", *J. Nucl. Mater.* 78, 2-16 (1978).
4. KLEINSCHMIDT P.D., D. CUBICCIOTTI and D.L. HILDENBRAND, "Thermodynamics of the Gaseous Zirconium Iodides", *J. Electrochem. Soc.* 125, 1543-1548 (1978).
5. CUBICCIOTTI D. and K.H. LAU, "Thermodynamics of Vaporization of  $ZrI_4$  from Substoichiometric Solid Zirconium Iodides", *J. Electrochem. Soc.* 126, 771-774 (1979).
6. CUBICCIOTTI D. and K.H. LAU, "Thermodynamics of Vaporization of  $ZrI_4$  in the Univariant Region: Zirconium Monoiodide/Zirconium", *J. Electrochem. Soc.* 128, 196-199 (1981).
7. SHIMADA S., T. MATSUURA and M. NAGAI, "Stress Corrosion Cracking of Zircaloy-2 by Metal Iodides", *J. Nucl. Sci. Technol.* 20, 593-602 (1983).
8. COX B., B.A. SURETTE and J.C. WOOD, "Stress Corrosion Cracking of Zircalloys in Unirradiated and Irradiated CsI", *J. Nucl. Mater.* 138, 89-98 (1986).
9. HARBOTTLE J.E., M.W. KENNARD, D.J. SUNDERLAND and A.A. STRASSER, "The Behaviour of Defective BWR Barrier and Non-Barrier Fuel", *Proceedings of the 1994 International Topical Meeting on Light Water Reactor Fuel Performance*, Florida, Amer. Nucl. Soc. 391-397 (1994).
10. SCHRIRE D., G. LYSELL, G. FRENNING, G. RONNBERG and A. JONSSON, "Secondary Defect Behaviour in ABB Fuel", *Proceedings of the 1994 International Meeting on Light Water Reactor Fuel Performance*, Florida, Amer. Nucl. Soc. 398-409, (1994).
11. GARAZOLLI F., R. VON JAN and H. STEHLE, "The Main Causes of Fuel Element Failure in Water-Cooled Power Reactors", *At. Energy Rev.* 17, 31-128, (1979).
12. WOOD J.C., B.A. SURETTE, I. AITCHISON and W.R. CLENDENING, "Pellet Cladding Interaction — Evaluation of Lubrication by Graphite", *J. Nucl. Mater.* 88, 81-94 (1980).
13. CHAN P.K. and K.J. KADDATZ, "CANLUB Development: Summary", *Proceedings of the 15th Annual Conference of the CNA/CNS, Montreal ...*(1994).
14. SMITH J.D. and J.D. CORBETT, "Stabilization of Clusters by Interstitial Atoms. Three Carbon-Centered Iodide Clusters,  $Zr_6I_{12}C$ ,  $Zr_6I_{14}C$  and  $MZr_6I_{14}C$  (  $M = K, Rb$  or  $Cs$ )", *J. Amer. Chem. Soc.* 107, 5704-5711 (1985).
15. CHEN T.M., S.M. KAUZLARICH and J.D. CORBETT, "Reactions and Products in the Cs-Zr-I-O System Relevant to Fission Product Chemistry—A Review", *J. Nucl. Mater.* 151, 225-237 (1988).
16. FLOYD M.R., J. NOVAK and P.T. TRUANT, "Fission-Gas Release in Fuel Performing to Extended Burnups in Ontario Hydro Nuclear Generating Stations", *AECL Report, AECL-10636*, 16p (1992).
17. CHAN P.K., K.G. IRVING, W.H. HOCKING, A.M. DUCLOS and A.F. GERWING, "Studies of Irradiated Zircaloy Fuel Sheath Using XPS", *Proceedings of the 16th Annual Conference of CNS/CNA, Saskatoon, AECL Report, AECL-11031*, 10p (1995).

18. ZHOU Y.N., M.R. FLOYD and M.A. RYZ, "Performance of Bruce Natural UO<sub>2</sub> Fuel Irradiated to Extended Burnups", Proceedings of the 4th International Conference on CANDU Fuel, Pembroke, AECL Report, AECL-11454, 9p (1995).
19. GERWING A.F., F.E. DOERN and W.H. HOCKING, "X-Ray Photoelectron Spectroscopy Using a McPherson ESCA-36 Equipped with an SSL Position-Sensitive Detector", Surf. Interface Anal. 14, 559-566 (1989).
20. HOCKING W.H., A.M. DUCLOS and L.H. JOHNSON, "Study of Fission-Product Segregation in Used CANDU Fuel by X-Ray Photoelectron Spectroscopy (XPS). II", J. Nucl. Mater. 209, 1-26 (1994).
21. ANTHONY M.T., and M.P. SEAH, "XPS: Energy Calibration of Electron Spectrometers", Surf. Interface Anal. 6, 95-106 (1984).
22. HOCKING W.H., R.A. VERRALL, P.G. LUCUTA and H.J. MATZKE, "Depth-Profiling Studies of Ion-Implanted Cesium and Rubidium in SIMFUEL and Uranium Dioxide", Radiat. Effects Defects Solids, 125, 299-321 (1993).
23. BEHNKE R., L.C. BROWN and A.K. McILWAIN, "Performance of the WNRE Shielded SEM", Proceedings of the 2nd International Conference on CANDU Fuel", Pembroke, 282-291 (1989).
24. WASYWICH K.M., W.H. HOCKING, D.W. SHOESMITH and P. TAYLOR, "Differences in Oxidation Behavior of Used CANDU Fuel During Prolonged Storage in Moisture-Saturated Air and Dry Air at 150°C", Nucl. Technol. 104, 309-329 (1993).
25. LIDE D.R., Editor, "CRC Handbook of Chemistry and Physics", 71st Edition, CRC Press Inc., Boca Raton (1990/91).
26. EBBINGHAUS G. and A. SIMON, "Electronic Structure of Rb, Cs and Some of Their Metallic Oxides Studied by Photoelectron Spectroscopy", Chem. Phys. 43, 117-133 (1979).
27. GARISTO N.C., L.H. JOHNSON and W.H. HOCKING, "An Instant-Release Source Term for the Assessment of Used Nuclear Fuel Disposal" Proceedings of the 2nd International Conference on CANDU Fuel, Pembroke, 352-368 (1989).
28. BRIGGS D. and M.P. SEAH, Editors, "Practical Surface Analysis by Auger and X-Ray Photoelectron Spectroscopy" Wiley, Chichester (1983).
29. MOULDER J.F., W.F. STICKLE, P.E. SOBOL and K.D. BOMBEN, "Handbook of X-Ray Photoelectron Spectroscopy", Edited by J. CHASTAIN and R.C. KING Jr., Physical Electronics, Eden Prairie (1995).
30. ESTRADÉ-SZWARKOPF H. and B. ROUSSEAU, "UPS and XPS Studies of Alkali-Graphite Intercalation Compounds", Synthetic Metals, 23, 191-198 (1988).
31. MORGAN W.E., J.R. VanWAZER and W.J. STEC, "Inner-Orbital Photoelectron Spectroscopy of the Alkali Metal Halides, Perchlorates, Phosphates and Pyrophosphates", J. Amer. Chem. Soc. 95, 751-755 (1973).
32. MOERS H., J.G. DILLARD, H. KLEWE-NEBENIUS, G. KIRCH, G. PFENNIG and H.J. ACHE, "Study of Fission Product Loaded Aerosols from Core Melting Experiments", Spectrochimica Acta, 39B, 1563-1566 (1984).
33. MOERS H., J.G. DILLARD, H. KLEWE-NEBENIUS, G. KIRCH, G. PFENNIG and H.J. ACHE, "XPS Study of Iodine Released in Core Melting Experiments", Surf. Interface Anal. 7, 22-28 (1985).

34. TYLER J.W., "Surface Analysis Using X-Ray Photoelectron Spectroscopy of Iodine Deposits on 17%Cr/12%Ni and Mild Steel Surfaces Oxidized in CO<sub>2</sub>/CH<sub>3</sub>I Gas Mixtures", *J. Nucl. Mater.* 161, 72-88 (1989).
35. KLEYKAMP H., "The Chemical State of the Fission Products in Oxide Fuels", *J. Nucl. Mater.* 131, 221-246 (1985).
36. SALANECK W.R., H.R. THOMAS, R.W. BIGELOW, C.B. DUKE, E.W. PLUMMER, A.J. HEEGER and A.G. MacDIARMID, "Photoelectron Spectroscopy of Iodine-Doped Polyacetylene", *J. Chem. Phys.* 72, 3674-3678 (1980).
37. BALOOCH M. and D.R. OLANDER, "Kinetic Study of Zirconium-Iodine Reaction by Modulated Molecular Beam Mass Spectrometry", *J. Electrochem. Soc.* 130, 151-157 (1983).
38. CORBETT J.D., "Core Photoelectron Shifts in Reduced Zirconium Halides. Relaxation Effects and Delocalized Metal-Metal Bonding", *Inorg. Chem.* 22, 2669-2672 (1983).
39. HWU S.J., R.P. ZIEBARTH, S. VonWINBUSH, J.E. FORD and J.D. CORBETT, "Synthesis and Structure of Double-Metal-Layered Scandium, Yttrium, and Zirconium Chloride, Carbides and Nitrides, M<sub>2</sub>Cl<sub>2</sub>C and M<sub>2</sub>Cl<sub>2</sub>N", *Inorg. Chem.* 25, 283-287 (1986).
40. HILL D.M., H.M. MEYER III and J.H. WEAVER, "Ba Oxides: Core Level Binding Energies and Defect-Related Fermi Level Pinning" *Surf. Sci.* 225, 63-71 (1990).
41. EVANS S., R.G. PRITCHARD and J.M. THOMAS, "Relative Differential Subshell Photoionization Cross-Sections (Mg K $\alpha$ ) from Lithium to Uranium" *J. Electron Spectrosc. Relat. Phenom.* 14, 341-358 (1978).
42. HORN K., S. KRAUSE, G. WEINBERG and K. BANGE, "Study of Protective Coatings Containing Zirconium Using Electron Spectroscopy for Chemical Analysis", *Thin Solid Films*, 150, 41-50 (1987).
43. NAKAO A., M. IWAKI, J. TAKAHASHI and K. TERASHIMA, "X-Ray Photoelectron Spectroscopy Study of Zirconium-Implanted Iron and Carbon-Implanted Zirconium", *Surf. Coatings Technol.* 66, 373-376 (1994).
44. ZHOU N. Private Communication (1996).
45. MATZKE H.J. "Radiation Damage in Crystalline Insulators, Oxides and Ceramic Nuclear Fuels", *Radiat. Effects*, 64, 3-33 (1982).
46. ZIEGLER J. "TRIM-95 Computer Code for Simulation of the Transport of Ions in Matter" (1995).
47. KROTO H.W., J.R. HEATH, S.C. O'BRIEN, R.F. CURL and R.E. SMALLEY, "C<sub>60</sub>: Buckminsterfullerene", *Nature*, 318, 162-163 (1985).
48. ELOI C.C., J.D. ROBERTSON, A.M. RAO, P. ZHOU, K.A. WANG and P.C. EKLUND, "An Investigation of Photoassisted Diffusion of Oxygen in Solid C<sub>60</sub> Films Using Resonant Alpha-Scattering", *J. Mater. Res.* 8, 3085-3089 (1993).

TABLE 1. POWER HISTORIES AND PIE DATA FOR CANDU FUELS

Fuel Bundle (Outer Element)	Burnup (MW·h/kg U)	Peak Power (kW/m)	Power History Type	Fission-Gas Release (%)	CANLUB Retention (%)
Y00005Z	212	45	Constant		
BDL-406-XY	560	33	Constant	2	18
BDL-406-AAH	715	37	Declining	2	7
BDL-406-GF	950	37	Constant	17	20

TABLE 2. CHEMICAL-SHIFT DATA FROM XPS ANALYSIS OF FUEL SHEATHS

Core Level or Auger	Energy (eV)		Core Level or Auger	Energy (eV)	
	Unspattered	Sputtered		Unspattered	Sputtered
Cs 3d <sub>3/2</sub>	738.62	738.80	Rb 3p <sub>1/2</sub>	247.18	247.41
Cs 3d <sub>5/2</sub>	724.62	724.82	Rb 3p <sub>3/2</sub>	238.20	238.49
Cs MNN	684.85	684.73	Rb 3d	110.45	110.61
Cs α'	1293.37	1293.69	I 3d <sub>3/2</sub>	630.51	630.62
Cs 4d <sub>3/2</sub>	77.60	77.77	I 3d <sub>5/2</sub>	619.01	619.15
Cs 4d <sub>5/2</sub>	75.57	75.75	Te 3d <sub>3/2</sub>	586.52	583.17
Ba 3d <sub>3/2</sub>	795.49	795.65	Te 3d <sub>5/2</sub>	576.34	572.88
Ba 3d <sub>5/2</sub>	780.18	780.45	Cd 3d <sub>3/2</sub>	412.06	411.95
Ba 4d <sub>3/2</sub>	92.22	92.56	Cd 3d <sub>5/2</sub>	405.36	405.22
Ba 4d <sub>5/2</sub>	89.48	89.97	Cl 2p	198.16	198.30

TABLE 3. QUANTITATIVE ANALYSIS OF NEAR SURFACE REGION BY XPS

Sputter Time	Composition (atom %) as a Function of Sputter Time (min)						
	0	1	3	8	20	40	80
Sheath #1							
C	60.5	68.8	72.5	71.2	67.4	68.5	67.9
O	22.9	15.9	13.4	15.4	16.9	16.0	16.9
Zr	0.70	0.90	0.88	1.06	1.13	1.13	1.20
Sn	0.24	0.23	0.22	0.18	0.14	0.09	0.04
Cs	11.1	9.68	8.59	7.72	9.18	8.75	8.94
Ba	0.26	0.43	0.44	0.46	0.70	0.74	0.78
Rb	0.40	0.27	0.20	0.23	0.23	0.19	0.24
I	0.95	1.15	1.11	1.43	2.62	2.73	3.08
Cl	2.28	1.88	1.84	1.43	0.61	0.63	
Te	0.15	0.18	0.14	0.13	0.10	0.18	0.18
U	0.46	0.62	0.67	0.82	0.98	1.02	0.80

TABLE 3. QUANTITATIVE ANALYSIS OF NEAR SURFACE REGION BY XPS (cont.)

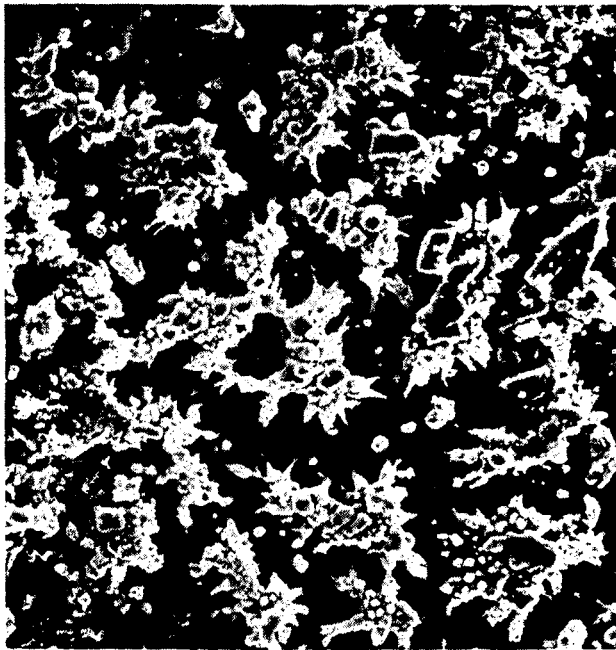
Composition (atom %) as a Function of Sputter Time (min)							
Sputter Time	0	1	3	8	20	40	80
Sheath #2							
C	57.6	54.1	56.6	48.8	44.9	46.2	46.0
O	18.1	19.1	17.7	24.3	31.4	32.1	33.8
Zr	0.59	1.06	1.17	1.36	2.37	2.60	3.09
Sn	0.25	0.35	0.35	0.44	0.45	0.38	0.19
Cs	16.0	17.5	16.1	16.0	13.2	11.7	9.72
Ba							0.10
Rb	0.32	0.27	0.26	0.29	0.29	0.28	0.25
I	0.43	0.55	0.61	0.79	1.31	1.44	1.71
Cl	5.47	5.34	5.20	5.14	1.95	0.80	
Te	0.34	0.28	0.32	0.39	0.22	0.15	0.11
U	0.85	1.41	1.68	2.50	3.84	4.37	5.10
Plenum Spacer							
C	66.5	67.1	70.5	66.1	65.1	64.1	60.2
O	21.6	19.3	17.2	20.0	20.6	22.1	25.3
Zr	2.18	2.95	3.05	3.97	4.47	4.87	6.47
Sn	0.04	0.13	0.12	0.10	0.11	0.11	0.11
Cs	6.10	6.07	5.32	5.45	4.84	4.34	3.93
Ba	0.32	0.35	0.37	0.43	0.48	0.51	0.58
Rb	1.02	1.01	0.86	0.80	0.77	0.47	0.42
I	0.52	0.64	0.64	0.97	1.06	1.09	1.13
Cl	0.75	1.06	0.75	0.77	0.85	0.71	
Te	0.50	0.68	0.58	0.47	0.62	0.48	0.56
Cd	0.20	0.18	0.19	0.21	0.19	0.20	0.11
U	0.29	0.48	0.50	0.74	0.90	0.99	1.15
End Cap							
C	64.6	66.6	69.9	69.1	66.9	66.9	64.1
O	22.9	19.6	16.8	16.8	18.3	18.4	21.6
Zr	0.78	1.12	1.12	1.58	2.29	3.14	4.71
Sn		0.06	0.05	0.07	0.06	0.03	0.03
Cs	3.93	4.38	4.10	4.34	4.17	4.06	3.74
Ba	0.48	0.52	0.56	0.71	0.81	0.90	1.07
Rb	5.80	5.67	5.14	5.01	4.34	3.75	3.54
I	0.40	0.50	0.46	0.57	0.63	0.60	0.55
Cl	0.94	1.28	1.40	1.35	1.91	1.63	
Te				0.07	0.11	0.07	0.14
Cd	0.08	0.12	0.14	0.16	0.19	0.16	0.11
U	0.08	0.15	0.17	0.23	0.29	0.33	0.42



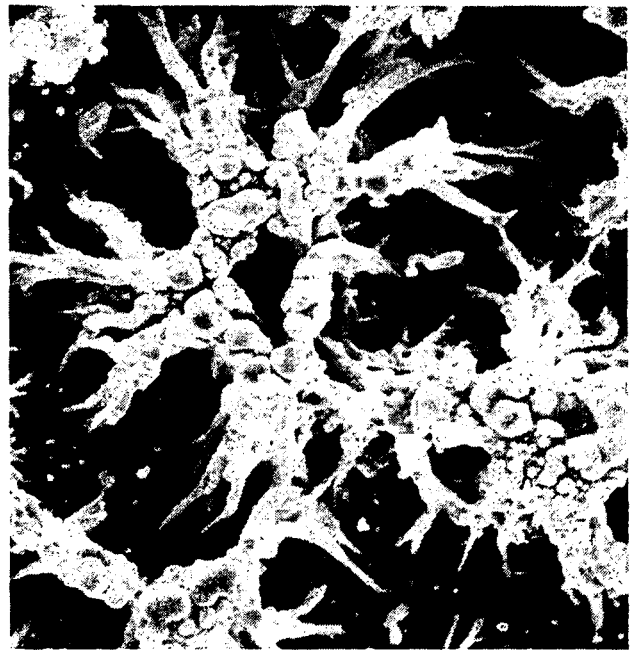
Y00005Z/4

60  $\mu\text{m}$ 

Y00005Z/4

12  $\mu\text{m}$ 

XY/11

12  $\mu\text{m}$ 

AAH/8

6  $\mu\text{m}$ 

FIGURE 1. SECONDARY ELECTRON IMAGES OF SHEATH SURFACES FROM THREE CANDU FUELS WITH INCREASING BURNUP (FROM Y00005Z/4 TO AAH/8)



GF/2 Sheath 2

30  $\mu\text{m}$ 6  $\mu\text{m}$ 

GF/2 Sheath 2

30  $\mu\text{m}$ 6  $\mu\text{m}$ 

FIGURE 2. SECONDARY ELECTRON IMAGES OF THE SURFACE OF SHEATH SAMPLE #2 FROM THE HIGH-BURNUP CANDU FUEL (BDL-406-GF/2).

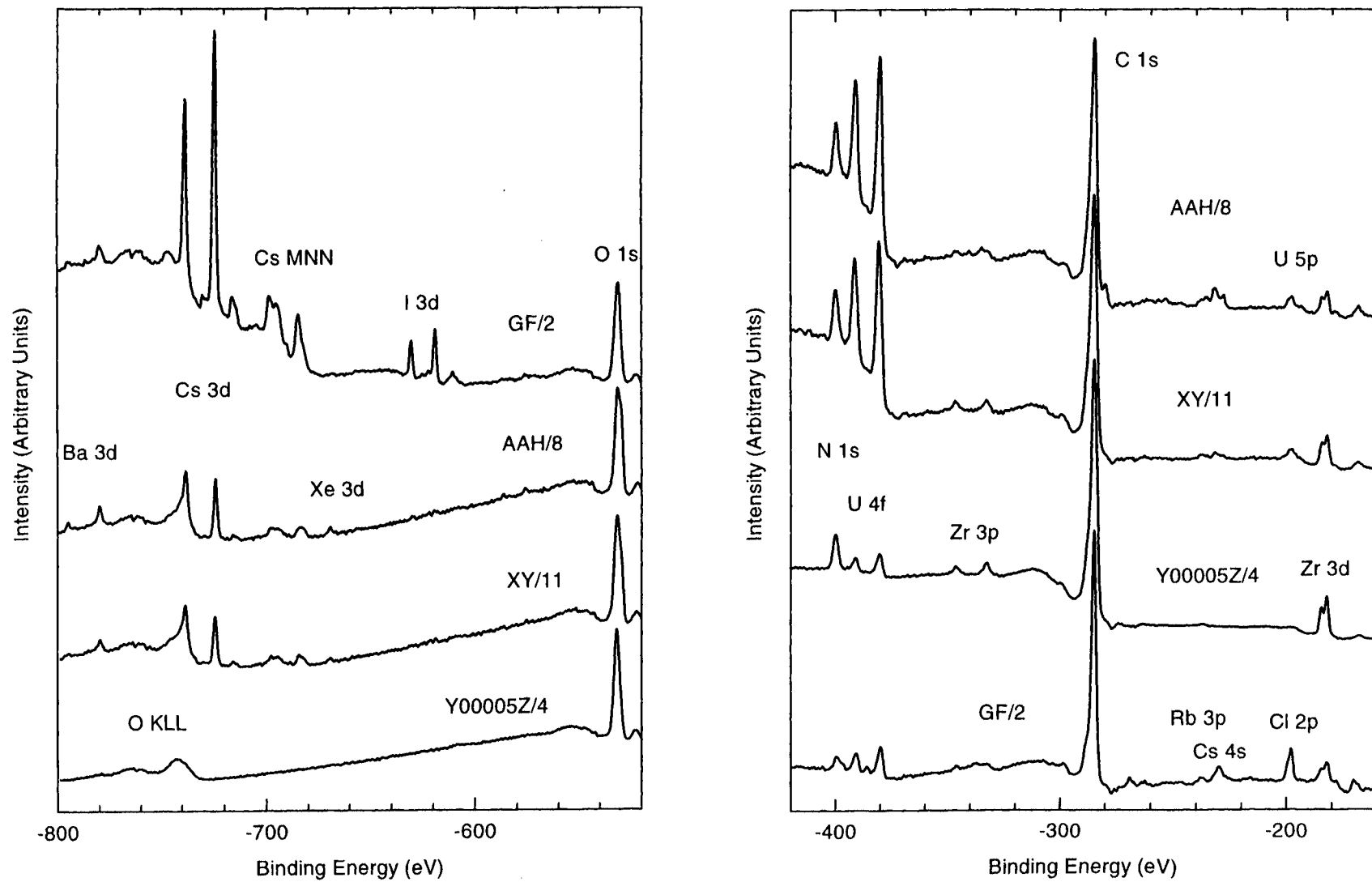


FIGURE 3. XPS SPECTRA COLLECTED FROM THE SHEATH/CANLUB SURFACES OF FOUR CANDU FUELS.

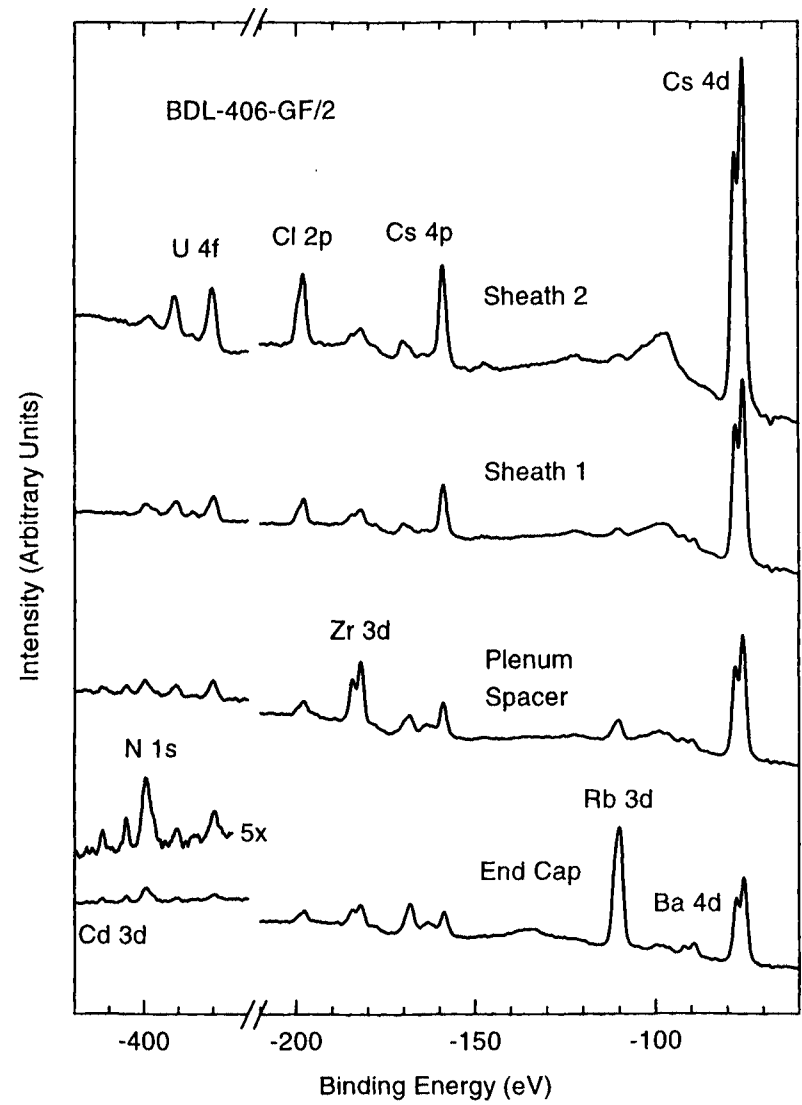
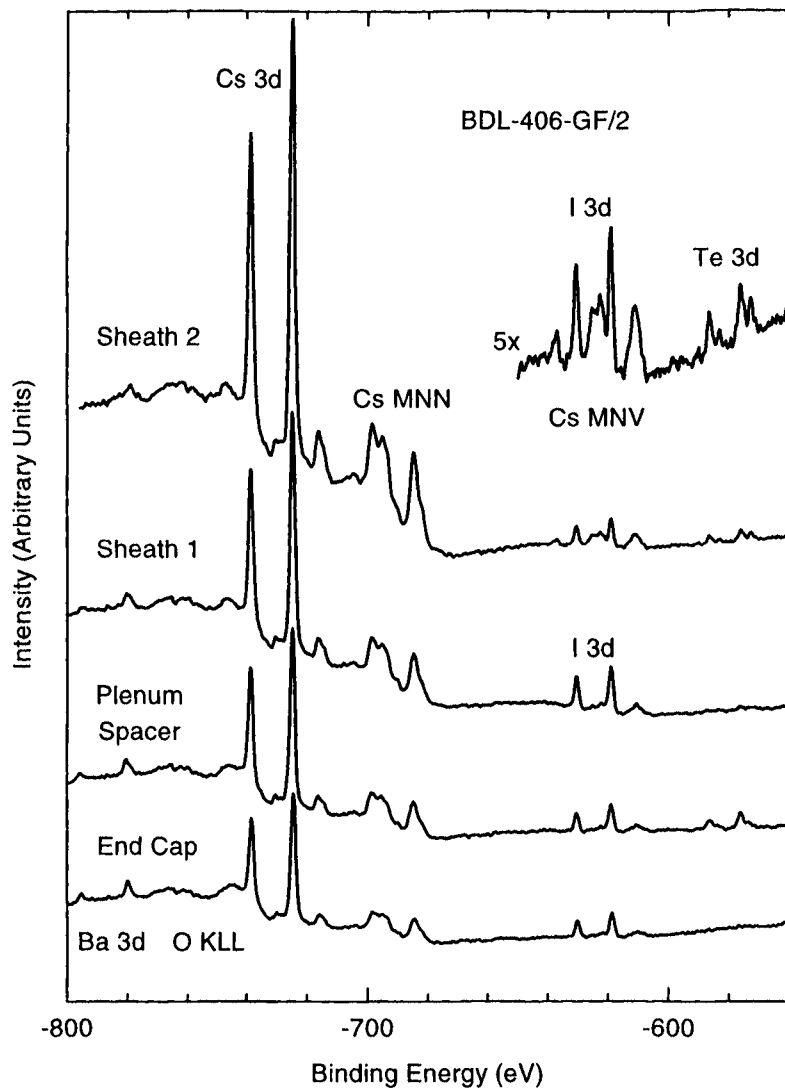


FIGURE 4. XPS SPECTRA RECORDED FROM SHEATH, PLENUM-SPACER AND END-CAP SURFACES OF THE HIGH-BURNUP CANDU FUEL.

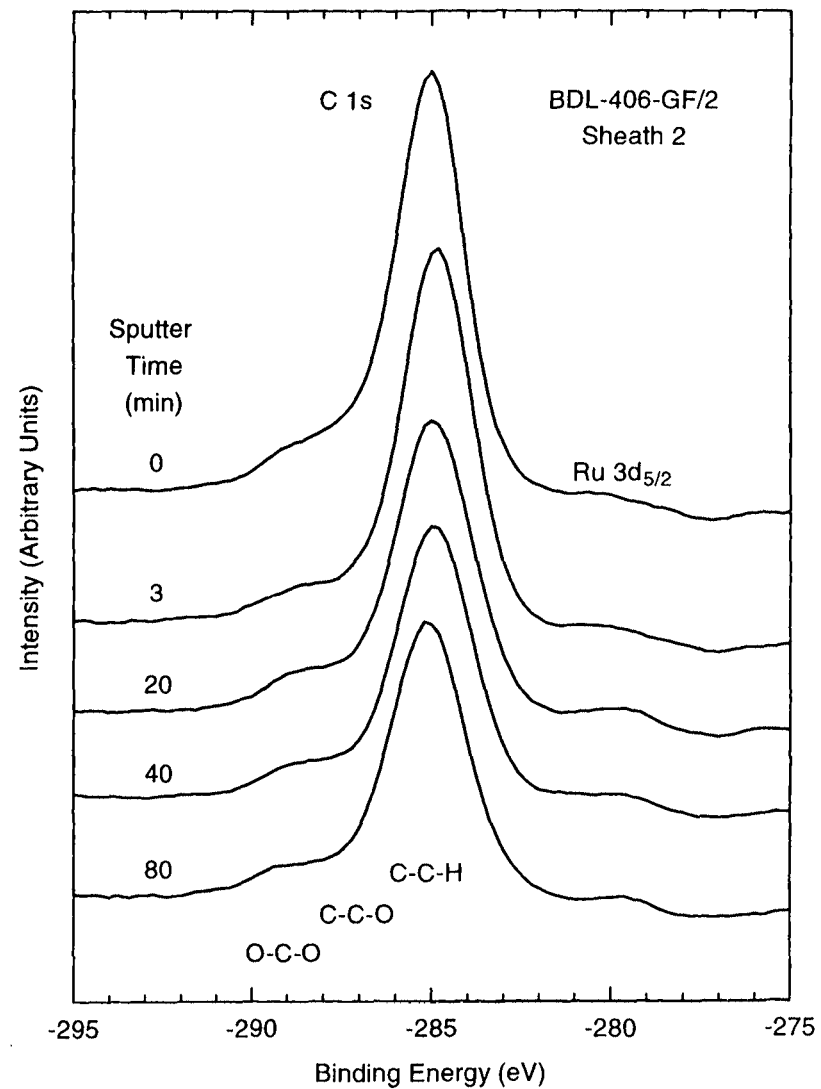
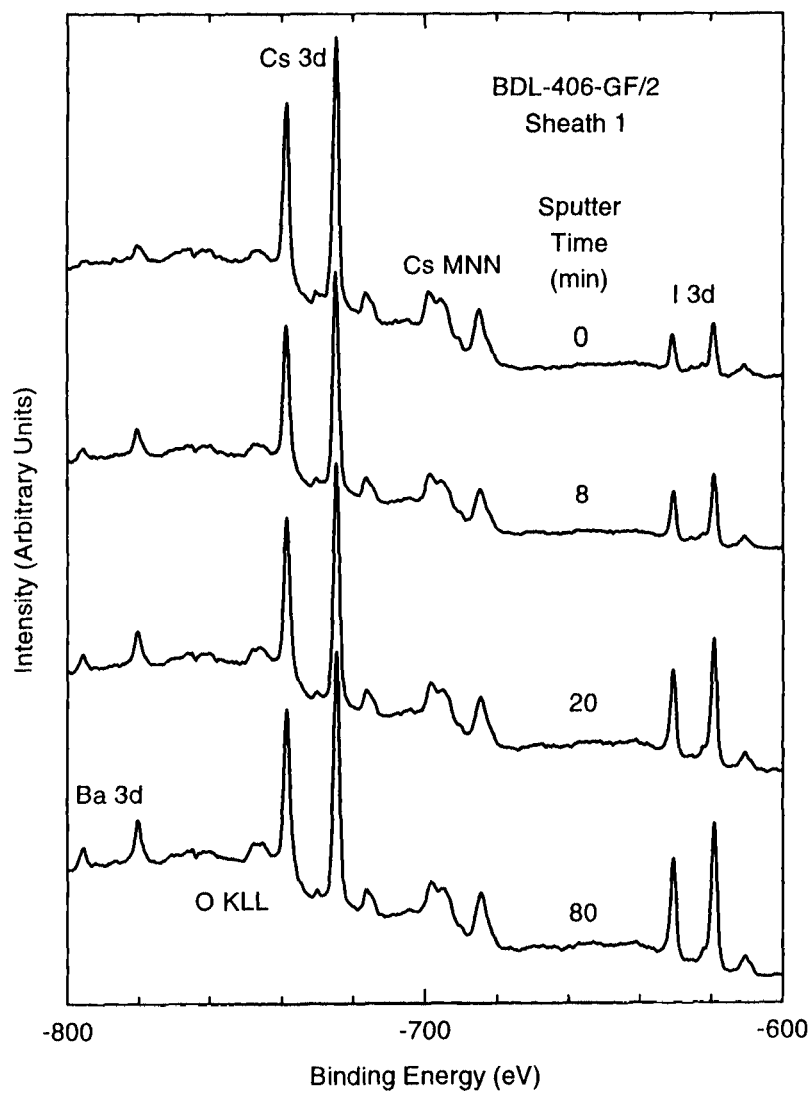


FIGURE 5. XPS SPECTRA RECORDED FROM SHEATH SURFACES OF THE HIGH-BURNUP CANDU FUEL AT DIFFERENT INTERVALS OF ARGON-ION SPUTTERING.

1  
2  
3  
4  
5  
6  
7  
8  
9  
10  
11  
12  
13  
14  
15  
16  
17  
18  
19  
20  
21  
22  
23  
24  
25  
26  
27  
28  
29  
30  
31  
32  
33  
34  
35  
36  
37  
38  
39  
40  
41  
42  
43  
44  
45  
46  
47  
48  
49  
50  
51  
52  
53  
54  
55  
56  
57  
58  
59  
60  
61  
62  
63  
64  
65  
66  
67  
68  
69  
70  
71  
72  
73  
74  
75  
76  
77  
78  
79  
80  
81  
82  
83  
84  
85  
86  
87  
88  
89  
90  
91  
92  
93  
94  
95  
96  
97  
98  
99  
100